

Supporting Information for the Manuscript

Characterizing Bonds Formed Between Platelet Factor 4 and Negatively Charged Drugs Using Single Molecule Force Spectroscopy

Stephan Block^{1,}, Andreas Greinacher², Christiane A. Helm³, Mihaela Delcea^{1,*}*

¹ZIK HIKE – Zentrum für Innovationskompetenz „Humorale Immunreaktionen bei kardiovaskulären Erkrankungen“, Fleischmannstr. 42 – 44, D-17489 Greifswald, Germany,

²Institut für Immunologie und Transfusionsmedizin; D-17475 Greifswald, Germany,

³Institut für Physik, Ernst-Moritz-Arndt Universität, Felix-Hausdorff-Str. 6, D-17487 Greifswald, Germany.

Tapping Mode Imaging – AFM images of PF4 coated mica surfaces were recorded using conventional Tapping Mode (TM) in air with standard tapping mode cantilevers (OMCL-AC160TS, $k \sim 40$ N/m, $f \sim 320$ kHz; purchased from Olympus, Hamburg, Germany). Before usage, cantilevers were tested with a Nioprobe self-imaging sample (Aurora Nanodevices, Nanaimo Canada) and only used for AFM imaging if the determined tip radius was significantly below 10 nm. In this study 512 x 512 pixels were recorded per image and the z -limit of the piezo scanner was set to 500 nm, in order to increase the height resolution of the AFM. The surface coverage of the PF4 was calculated from height histograms of the TM images. Only those SMFS measurement series, which had a PF4 surface coverage $>50\%$ on the mica, were included in the final data analysis (see Fig. S1).

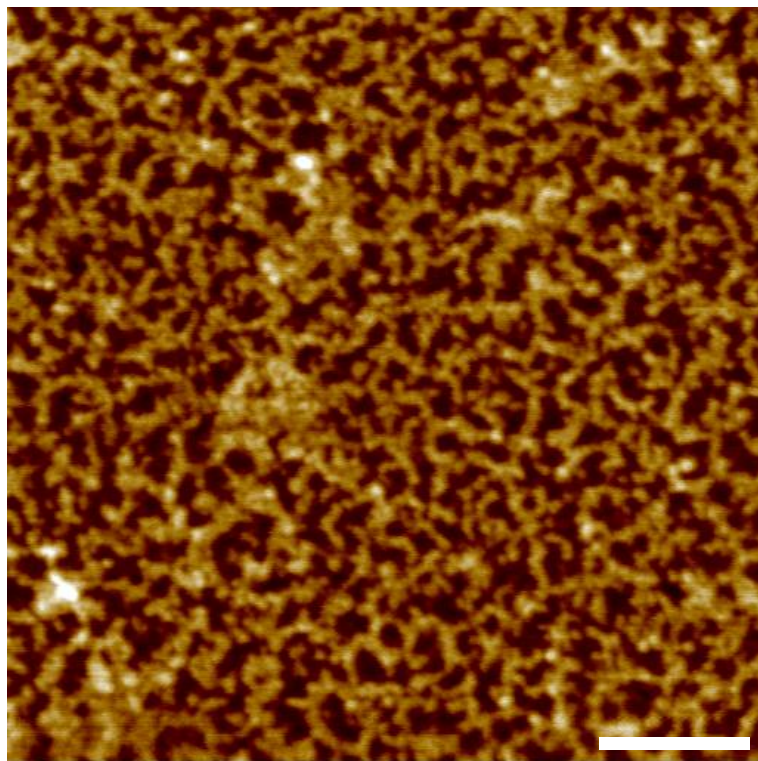


Fig. S1: Tapping mode AFM image of PF4-coated mica with a surface coverage of 65%. Scale bar: 200 nm, z -scale: 4 nm.

Unspecific events - Due to the experimental setup, the only sources of unspecific bonds are (i) GAG chains bound to uncoated parts of the mica (see Fig. 2c in the manuscript), or (ii) an AFM tip that is directly bound to PF4 (Fig. 2e in the manuscript). To estimate the amount of these unspecific events (which are not related to GAG/PF4 unbinding), two control experiments have been performed: (i) interaction of a GAG-functionalized AFM tip with a bare, freshly cleaved mica surface (Fig. 2c in the manuscript), and (ii) interaction of a non-functionalized AFM tip with a PF4 coated surface (Fig. 2e in the manuscript).

For the first control experiment, GAG-functionalized AFM tip interacting with a freshly cleaved mica surface, we observe in ~60% of the force curves rupture events, which show a force plateau (*i.e.*, a constant force) instead of an force that increases with chain stretching (see Fig. 2d in the manuscript). Hence, these events cannot be fitted with the mFJC model and are attributed to sliding of GAG chains on the bare mica. Only ~5% of these force curves contained events that can be fitted using the mFJC model. The remaining 35% contained neither chain sliding nor stretching-like events.

However, as the majority of the force curves of this control experiment contains sliding events, which can be unambiguously identified by their force plateaus, it is possible to estimate the amount of rupture events originating from the unspecific interaction of GAG chains with bare mica in the SMFS experiments. On average, only 2.5% of the force curves (involving GAG/PF4-bond rupture) contain sliding events, so that not more than 5% of these force curves can originate from unspecific interaction of GAG chains with bare mica.

For the second control experiment, bare AFM tip interacting with a PF4-coated mica surface, we observed adhesion in all force curves and in less than 10% of the force curves events that can be fitted using the mFJC model (see Fig. 1f in the manuscript). However, as the fitted contour

lengths L_C are generally smaller than 8 nm for these unspecific events, they can be completely excluded from data analysis by restricting to events having fitted contour lengths $L_C > 8$ nm.

This procedure allows to exclude unspecific events from the interaction of a bare AFM tip with PF4-coated mica. Hence, the only source of unspecific events is the interaction of GAG chains with bare mica, which creates less than 5% of the events observed in the SMFS experiments on GAG/PF4-bond rupture.

SMFS Parameters – Tables S1 and S2 contain the GAG/PF4-bond parameters extracted from the SMFS experiments. For Table S1 the data analysis was conducted on all SMFS data points, while for Table S2 the data analysis was restricted to the “dense cloud” of data points (see Fig. 2 in the manuscript), which excludes events attributed to simultaneous rupture of 2 GAG/PF4-bonds. As this procedure excludes only a small amount of events (<15% for chondroitin sulfate A, <10% for unfractionated heparin, <5% for dextran sulfate), both approaches lead to very similar values in the SMFS parameters: reaction coordinate x_0 , bond lifetime in absence of any force τ_0 , and unbinding energy barrier ΔG .

all data points	$x_0 / \text{Å}$	$\nu = 1/2$		$\nu = 2/3$	
		τ_0 / s	$\Delta G / k_B T$	τ_0 / s	$\Delta G / k_B T$
chondroitin sulfate A	1.86	0.21	-0.57	0.044	-0.78
unfractionated heparin	2.30	0.18	-0.78	0.041	-0.93
dextran sulfate	2.18	0.09	-0.45	0.018	-0.96
average	2.11±0.23	0.16±0.06	-0.60±0.17	0.034±0.014	-0.89±0.09

Table S1: SMFS parameters, if all SMFS data points are included in the data analysis.

dense cloud	$x_0 / \text{Å}$	$\nu = 1/2$		$\nu = 2/3$	
		τ_0 / s	$\Delta G / k_B T$	τ_0 / s	$\Delta G / k_B T$
chondroitin sulfate A	2.05	0.10	-0.93	0.024	-1.44
unfractionated heparin	2.39	0.13	-1.05	0.030	-1.38
dextran sulfate	2.22	0.09	-0.54	0.017	-1.32
average	2.22±0.17	0.11±0.02	-0.84±0.27	0.024±0.007	-1.38±0.06

Table S2: SMFS parameters when SMFS data points (attributed to simultaneous rupture of 2 GAG/PF4-bonds) are excluded from the data analysis.

SMFS Parameter Plots

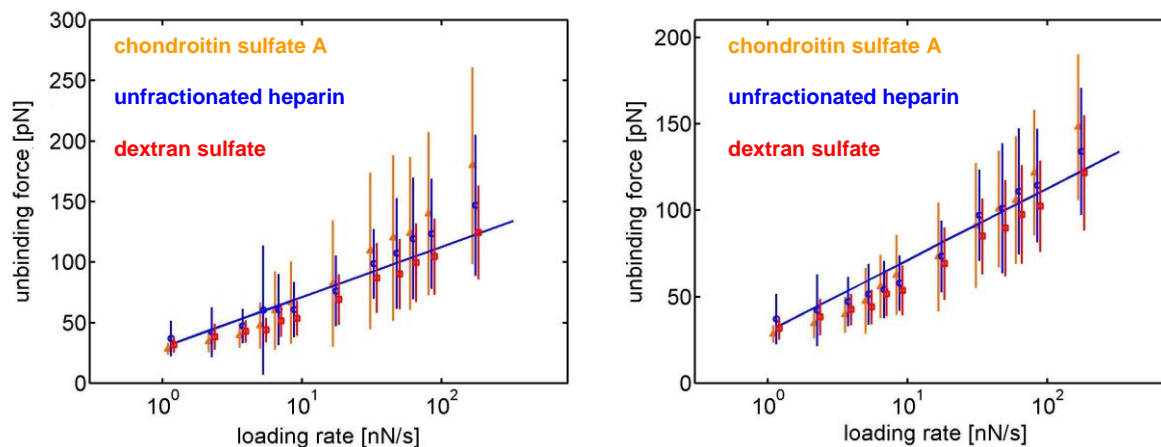


Fig. S2: Loading rate dependent rupture forces of PF4/GAG-bonds for chondroitin sulfate A (orange triangles), UFH (blue circles), and dextran sulfate (red squares). For the **left** figure the data analysis was conducted on all SMFS data points, while for the **right** one the data analysis was restricted to the “dense cloud” of data points, which excludes events attributed to simultaneous rupture of 2 GAG/PF4-bonds. In both cases, no statistically significant deviations between the different GAGs were observed. The blue line gives a LMS fit of Eq. 4 to the UFH data.

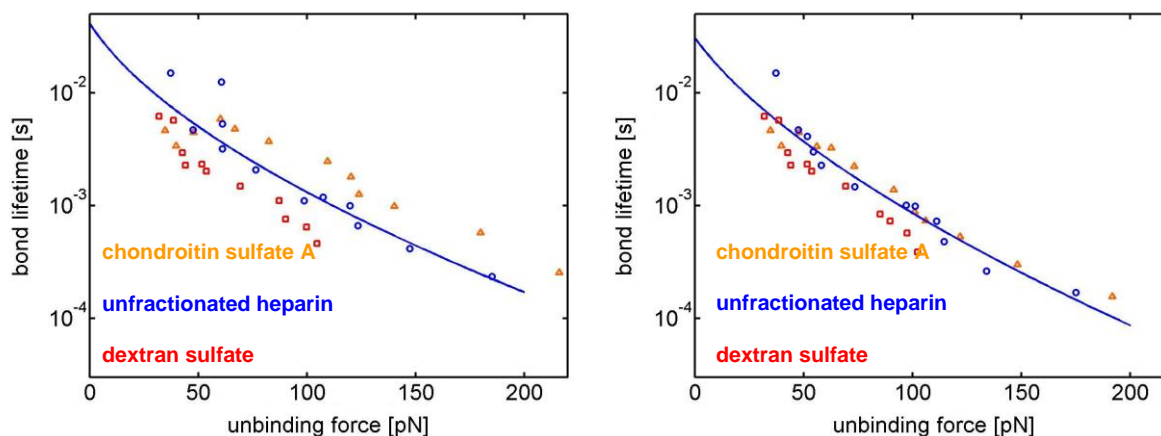


Fig. S3: PF4/GAG-bond lifetime calculated using Eq. 2 for chondroitin sulfate A (orange triangles), UFH (blue circles), dextran sulfate (red squares). For the **left** figure the data analysis was conducted on all SMFS data points, while for the **right** one the data analysis was restricted to the “dense cloud” of data points, which excludes events attributed to simultaneous rupture of 2 GAG/PF4-bonds. Including those events (**left**) increases the apparent scattering of the unbinding force, which slightly decreases the bond lifetime. As chondroitin sulfate A contains more of those events than unfractionated heparin and dextran sulfate, the bond lifetimes shift slightly to smaller values (**left**), which is not observed if these events are excluded from the data analysis (**right**). However, this small (erroneous) shift in τ is still too small to be statistically relevant. Hence, in both cases we again observe no significant deviations between the different GAGs.

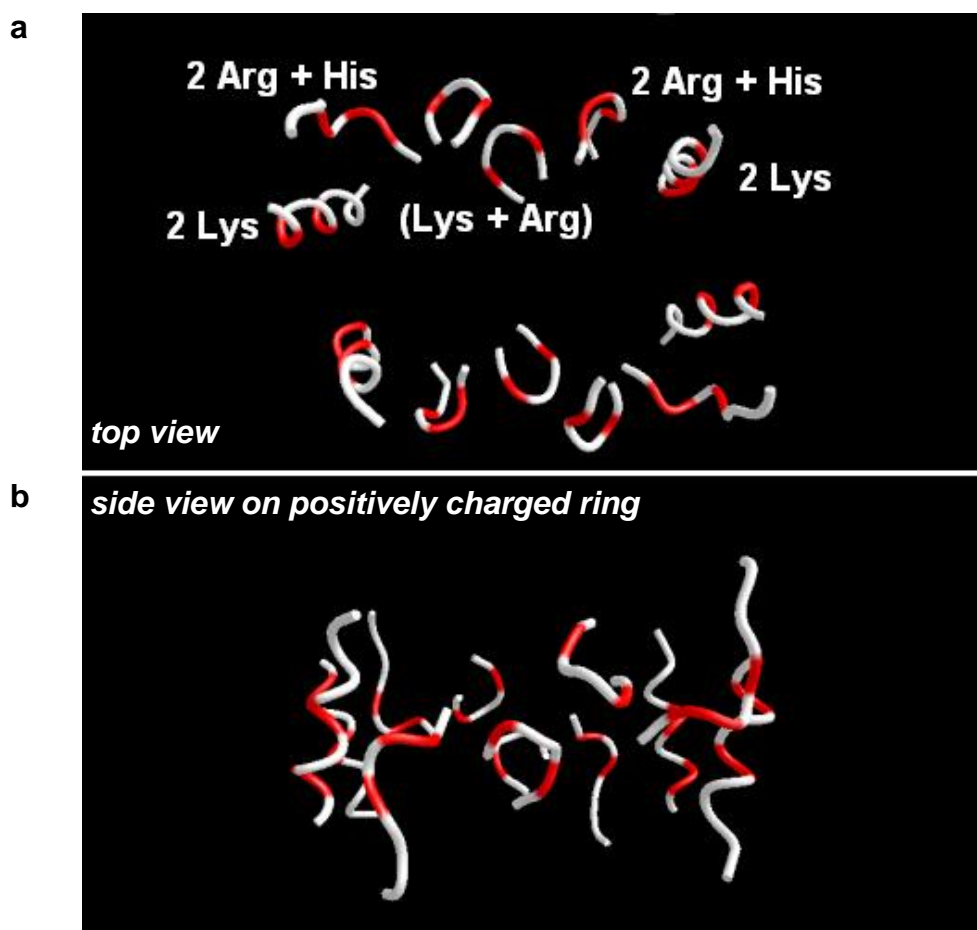


Fig. S4: Molecular model of the PF4 protein structure as determined by x-ray crystallographic measurements of Zhang et al.⁴¹ (code 1RHP of the Brookhaven Protein Data Bank). The view axis in (a) is perpendicular to the plane of the PF4/heparin-binding site (giving a “top view” on this plane), while in (b) a side view on this plane was chosen. Shown are only the positively charged amino acids involved in heparin binding (as judged from NMR measurements; red structures)³⁶ and the amino acids in their direct vicinity (white structures). Typically, amino acids involved in heparin binding are paired with a typical distance of 0.9 nm perpendicular to the binding plane and of 0.9 – 1.3 nm between the different AA pairs (*i.e.*, along the direction of the GAG binding course).

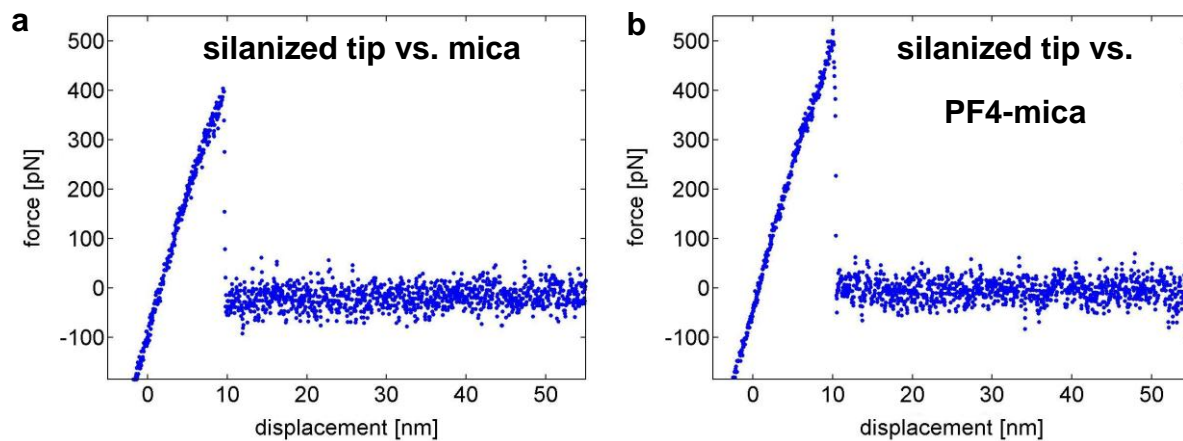


Fig. S5: Representative force profiles for the interaction of a silanized tip with (a) bare mica and with (b) PF4-functionalized mica. All such force profiles contain only a single surface adhesion event and none contained events that were similar to chain stretching or sliding (as for example seen for GAG-functionalized tips).

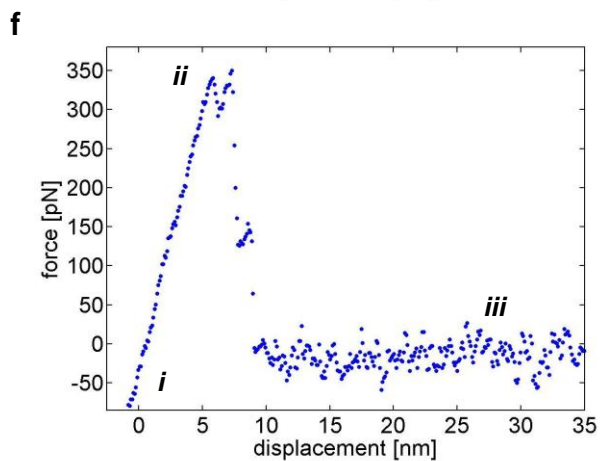
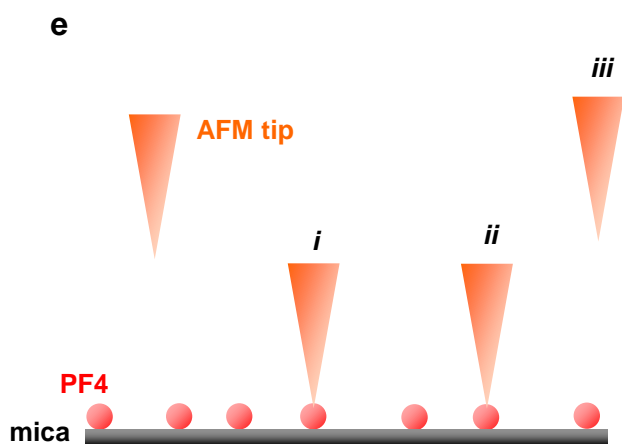
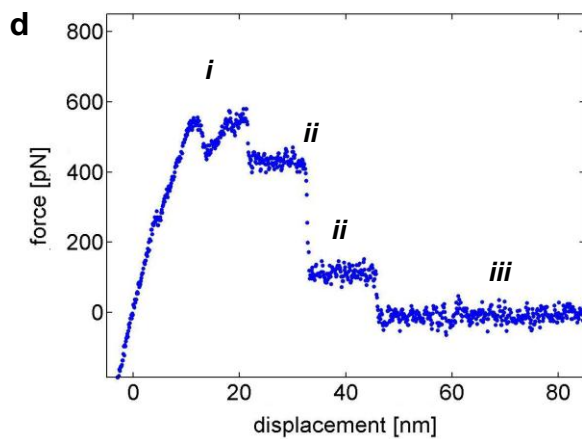
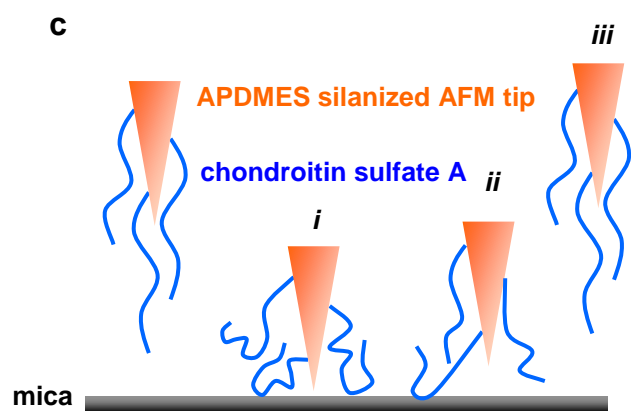
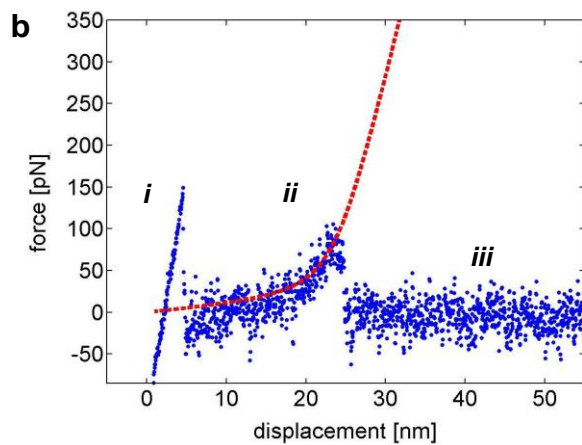
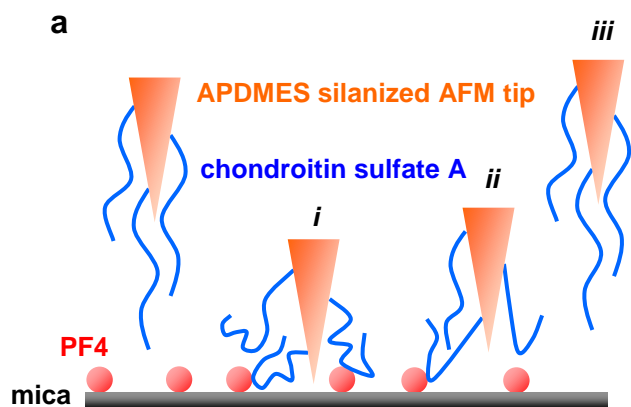


Fig. S6: Version of Fig. 2 for chondroitin sulfate A. **(a)** Setup of the SMFS measurements on platelet factor 4 (PF4) bound to chondroitin sulfate A and **(b)** a representative force curve recorded for this setup. **(c, d)** interaction of chondroitin sulfate A with bare mica and **(e, f)** interaction of a non-functionalized AFM tip with PF4 coated mica (same as Fig. 2e, f). The unspecific chondroitin sulfate A/mica interaction **(c, d)** is characterized by events that cannot be fitted by the mFJC model (**i**, adhesion peak + stretch-like events; **ii**, force plateaus, indicative for chondroitin sulfate A chain sliding on the mica surface), which are automatically excluded from data analysis. For the unspecific tip/PF4-interaction **(e, f)** only few force curves (<10%) contain events that may be fitted using the mFJC model. They typically show a very short ranged interaction (<8 nm) so that they can be excluded from data analysis by including only mFJC fits having apparent contour lengths >8 nm.

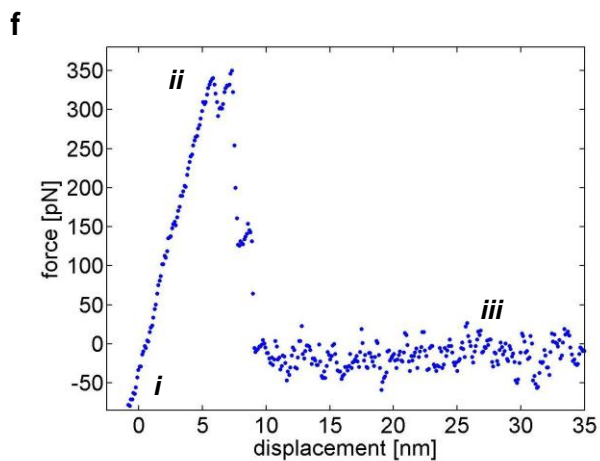
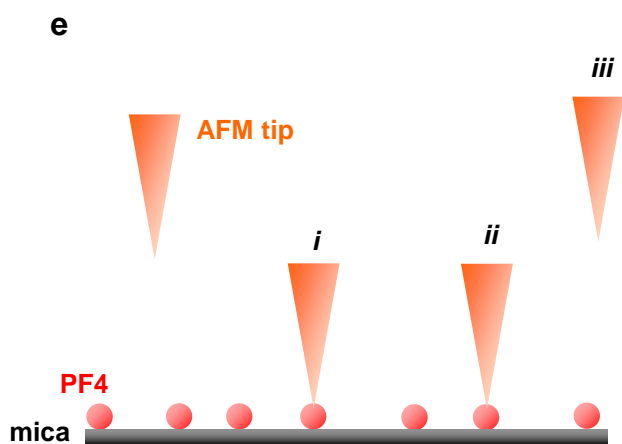
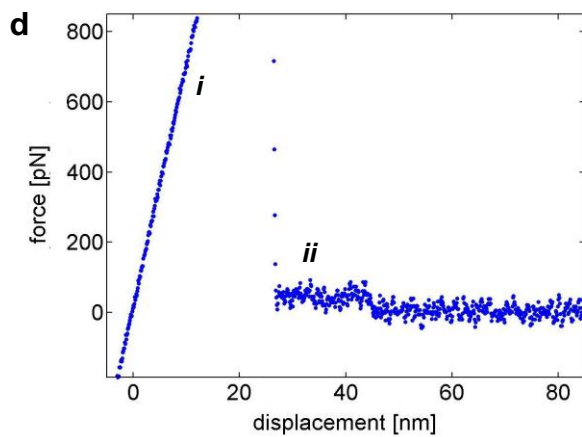
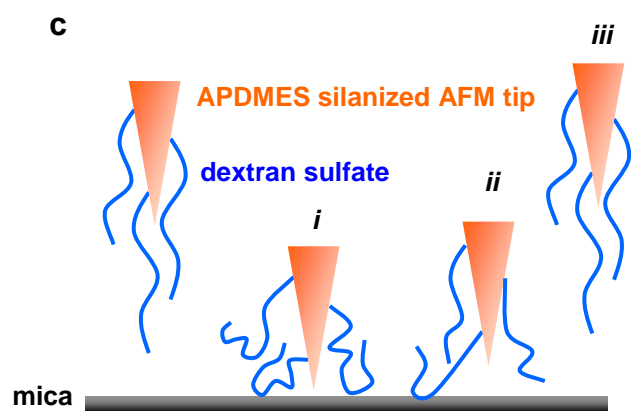
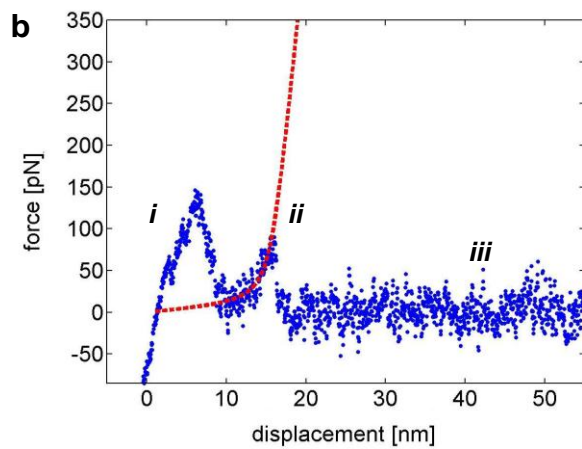
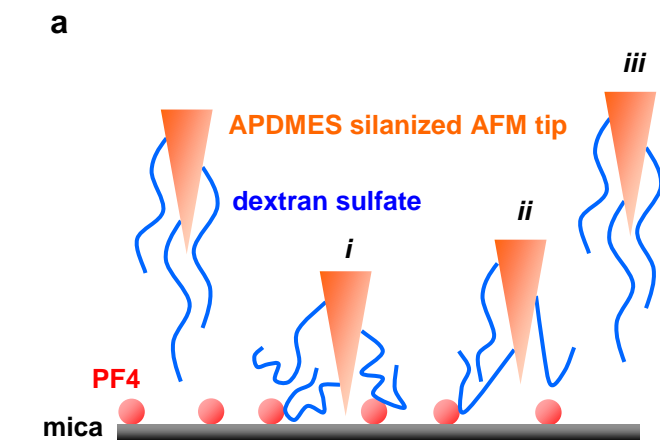
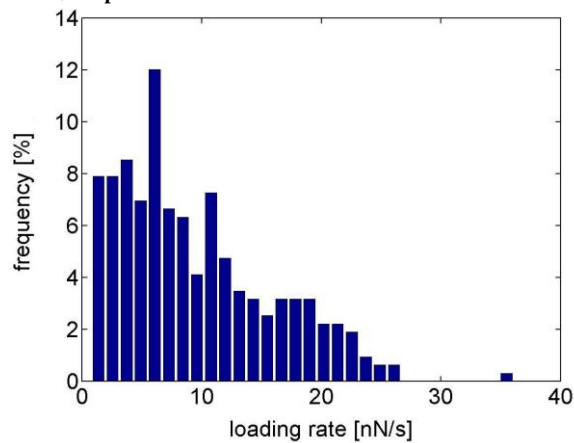
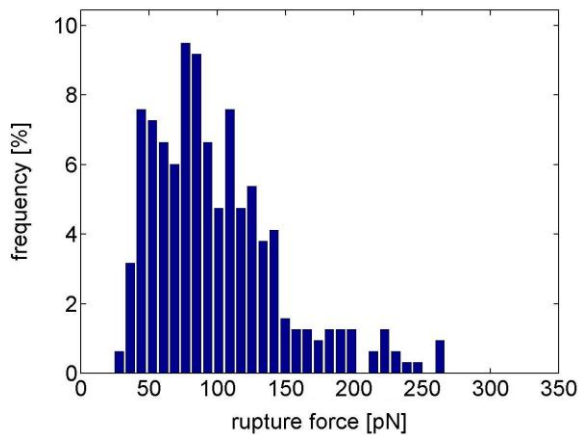
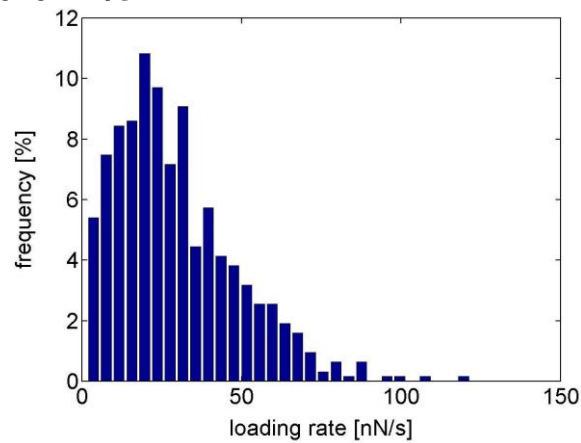
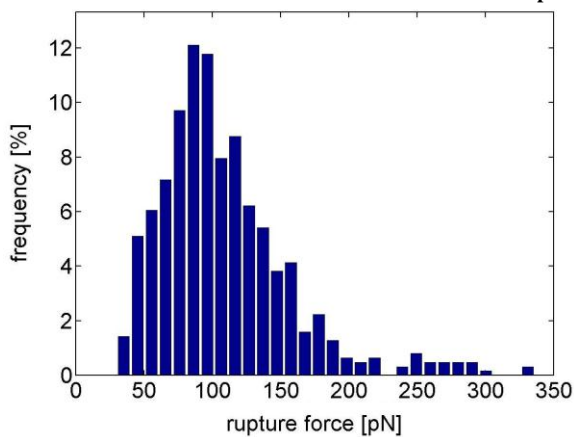


Fig. S7: Version of Fig. 2 for dextran sulfate. **(a)** Setup of the SMFS measurements on platelet factor 4 (PF4) bound to dextran sulfate and **(b)** a representative force curve recorded for this setup. **(c, d)** interaction of dextran sulfate with bare mica and **(e, f)** interaction of a non-functionalized AFM tip with PF4 coated mica (same as Fig. 2e, f). The unspecific dextran sulfate/mica interaction **(c, d)** is characterized by events that cannot be fitted by the mFJC model (**i**, adhesion peak; **ii**, force plateaus, indicative for dextran sulfate chain sliding on the mica surface), which are automatically excluded from data analysis. For the unspecific tip/PF4-interaction **(e, f)** only few force curves (<10%) contain events that may be fitted using the mFJC model. They typically show a very short ranged interaction (<8 nm) so that they can be excluded from data analysis by including only mFJC fits having apparent contour lengths >8 nm.

chondroitin sulfate A, $v_{\text{tip}} = 358 \text{ nm/s}$



$v_{\text{tip}} = 1070 \text{ nm/s}$



$v_{\text{tip}} = 2790 \text{ nm/s}$

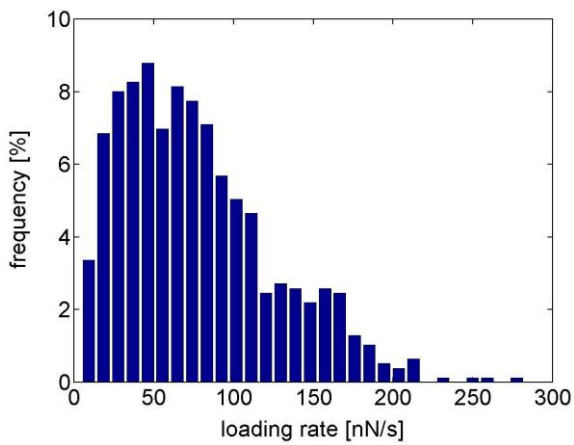
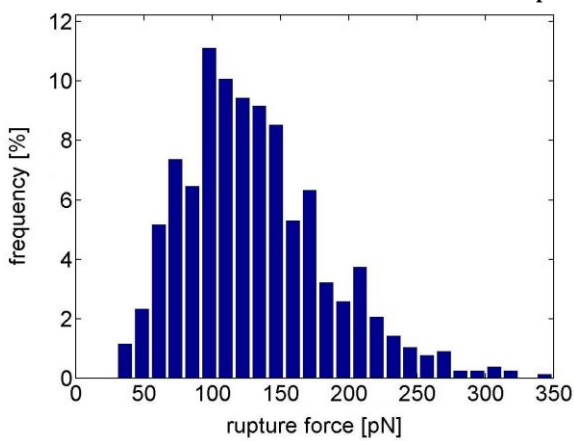


Fig. S8: Histograms of (**left column**) rupture force and (**right column**) loading rate distribution for the chondroitin sulfate A/PF4-interaction, conducted at the tip retraction velocities v_{tip} as indicated in the figures. The loading rate has always a broad distribution (containing small values even at large v_{tip}) making it necessary to group the measured events as described in the Materials and Methods section to extract meaningful values (the result can be found in Fig. S9).

chondroitin sulfate A

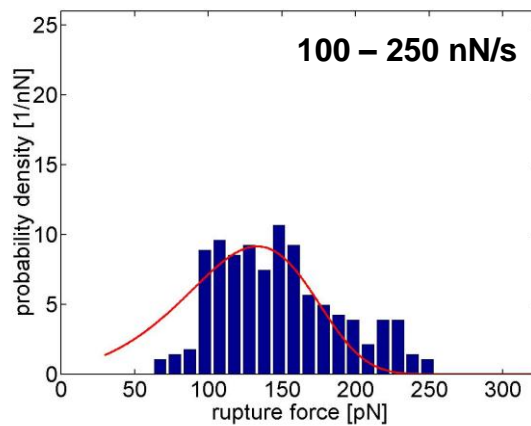
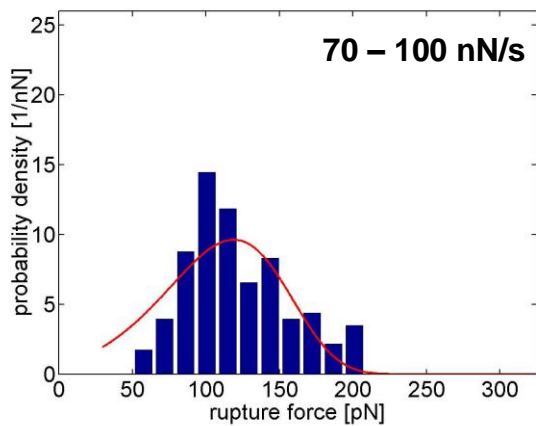
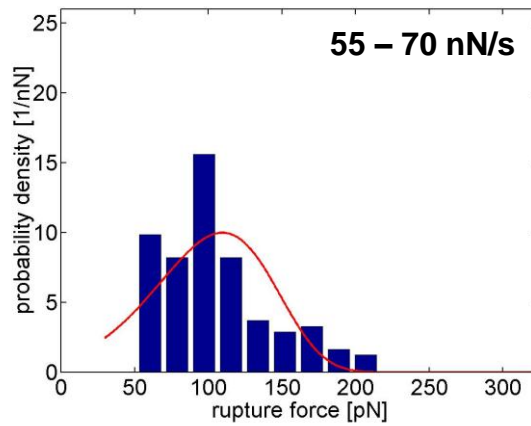
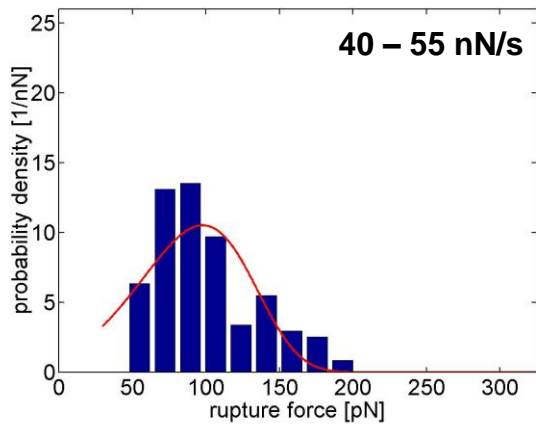
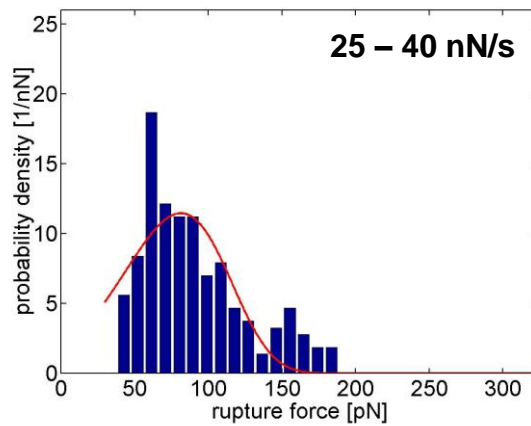
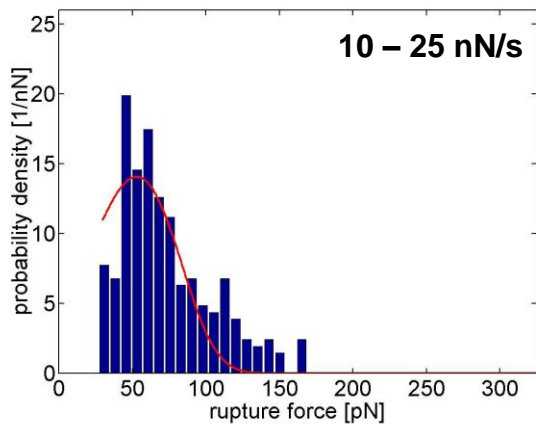


Fig. S9: Histograms of rupture force of the chondroitin sulfate A/PF4-interaction after grouping the events according to the loading rate (as described in the Materials and Methods section). Shown are only the loading rate intervals that contained enough data points to plot a histogram. The red line gives the theoretically expected probability distribution of the rupture force $w(F_u)$, if the binding parameters of chondroitin sulfate A (see Tab. S2) are inserted into the equation

$$w(F_u) = \frac{\exp\left(-\int_0^{F_u} (p \cdot \tau(F))^{-1} dF\right)}{p \cdot \tau(F_u)}, \quad (\text{S1})$$

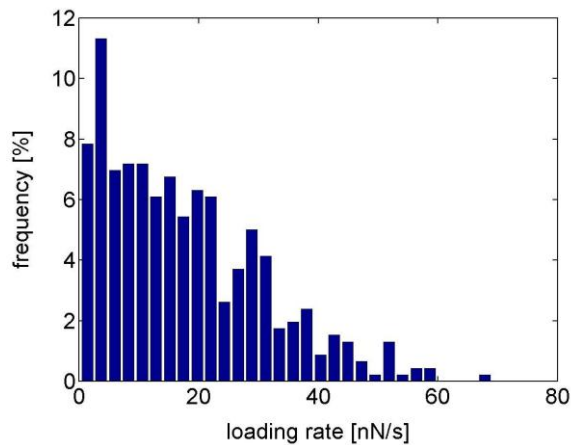
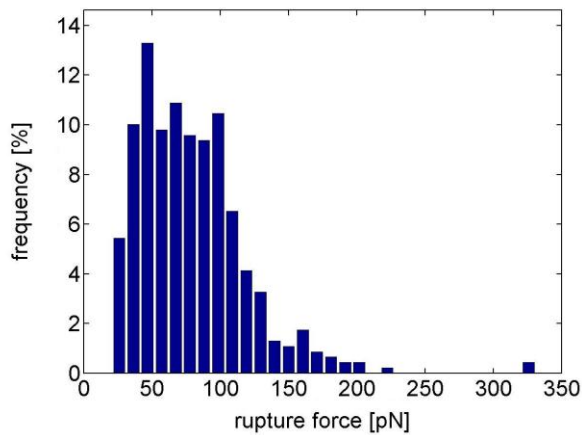
with p denoting the loading rate (indicated in the plots) and $\tau(F)$ the lifetime of a bond that is subject to a pulling force F (see Eq. 3 in the manuscript).[#] The experimentally and theoretically derived probability distributions of $w(F_u)$ are normalized to fulfil

$$\int_0^{\infty} w(F_u) dF_u = 1,$$

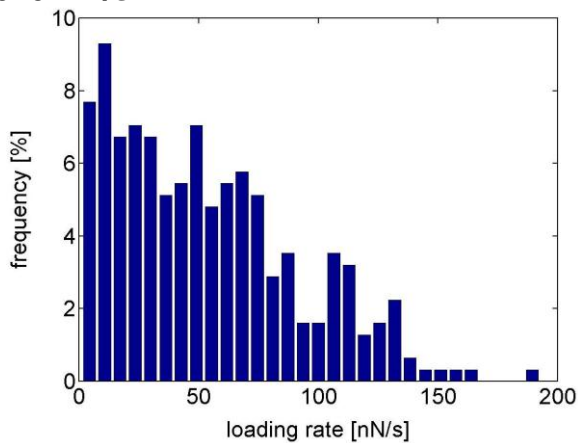
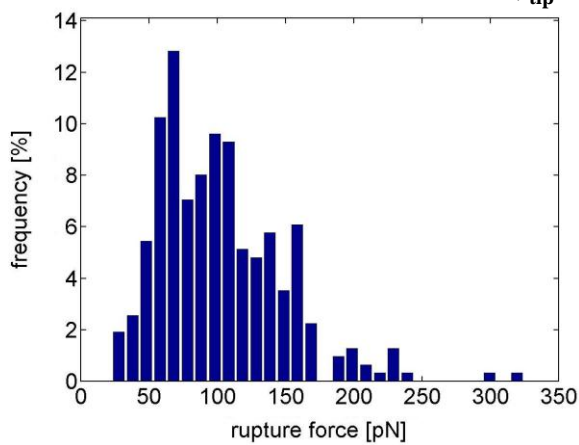
i.e., the peak height of the theoretically derived distribution comes directly from Eq. S1 and was not additionally adjusted (*e.g.*, by coupling the peak height of the theoretically derived distribution to the measured one). Although these histograms did not enter the data analysis, a good agreement between the experimentally and theoretically derived probability distributions is observed using only 3 binding parameters, showing that the data analysis creates self-consistent results.

[#] Dudko, O. K.; Hummer, G.; Szabo, A. Theory, analysis, and interpretation of single-molecule force spectroscopy experiments. *PNAS* **2008**, *105*, 15755-15760.

UFH, $v_{\text{tip}} = 358 \text{ nm/s}$



$v_{\text{tip}} = 1070 \text{ nm/s}$



$v_{\text{tip}} = 2790 \text{ nm/s}$

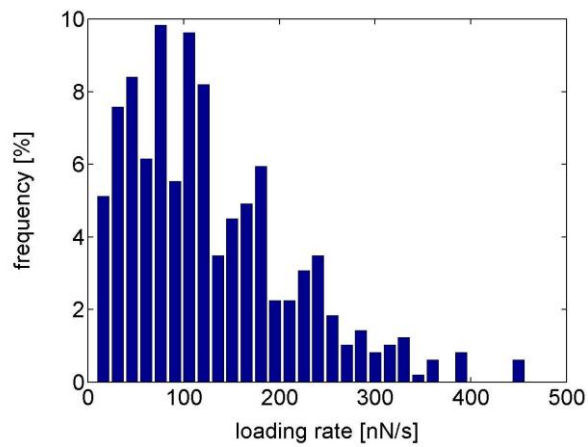
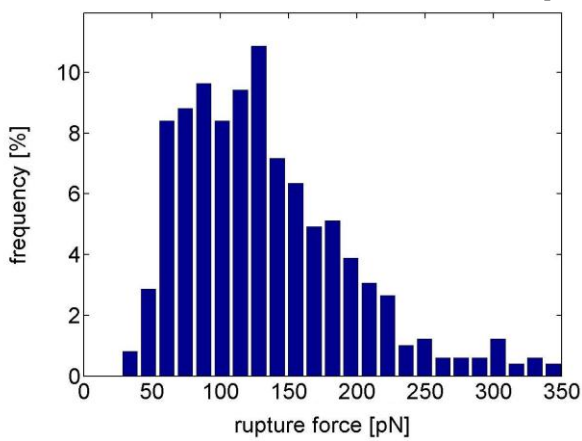


Fig. S10: Histograms of (**left column**) rupture force and (**right column**) loading rate distribution for the interaction of PF4 with unfractionated heparin (UFH), conducted at the tip retraction velocities v_{tip} as indicated in the figures. The loading rate shows always a broad distribution (containing small values even at large v_{tip}), making it necessary to group the measured events as described in the materials and methods section to extract meaningful values (the result can be found in Fig. S11).

UFH

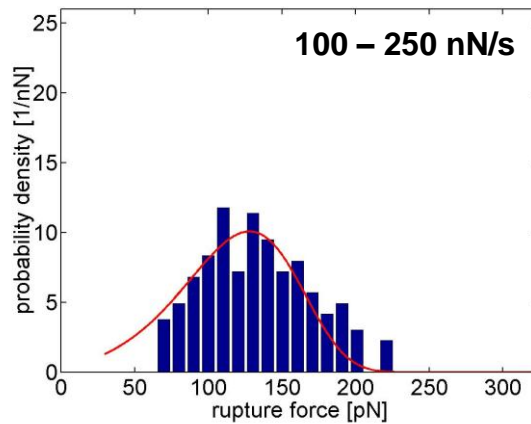
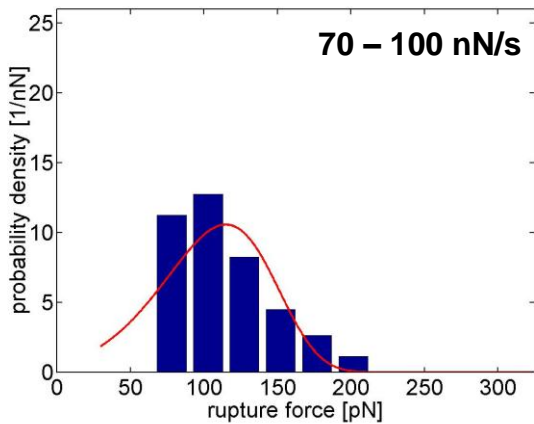
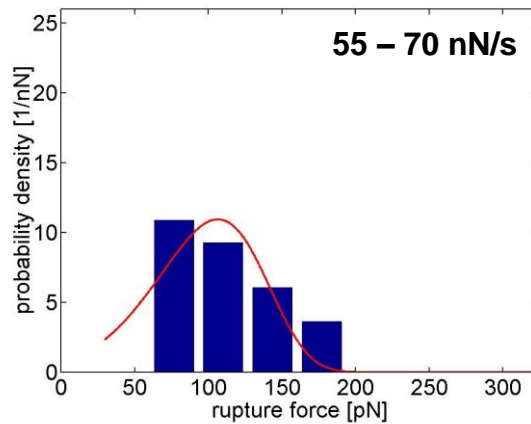
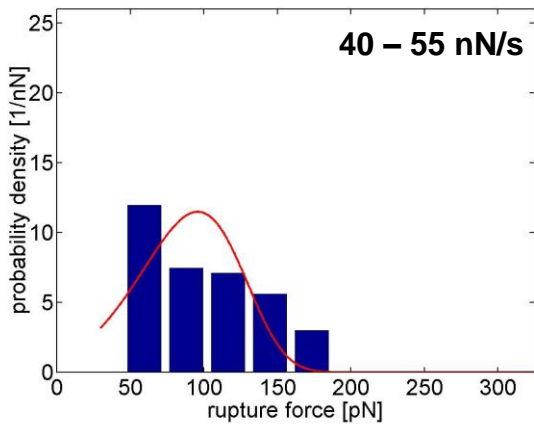
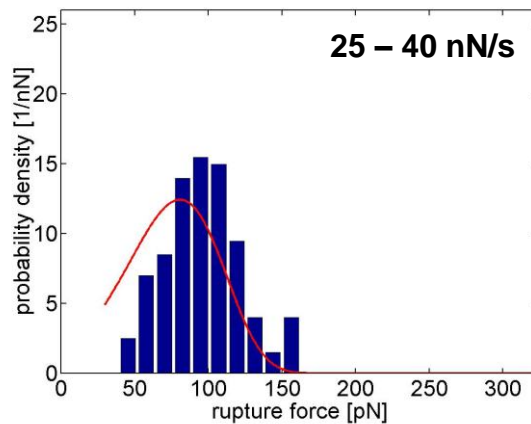
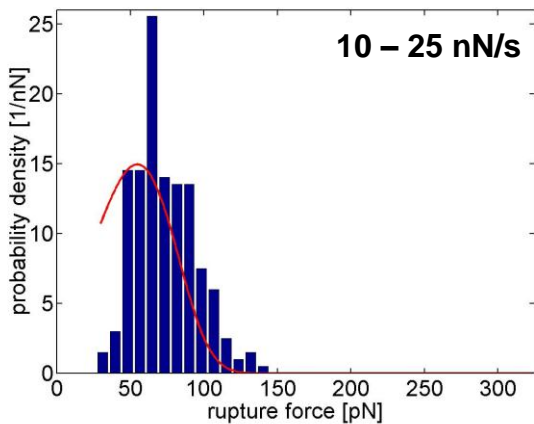


Fig. S11: Histograms of rupture force of the UFH/PF4-interaction after grouping the events according to the loading rate (as described in the Materials and Methods section). Shown are only the loading rate intervals that contained enough data points to plot a histogram. The red line gives the theoretically expected distribution of the rupture force $w(F_u)$ using the binding parameters of UFH (see Tab. S2) as described in Fig. S9. Minor deviations are found for low loading rates, while a very good agreement is observed for loading rates > 40 nN/s.

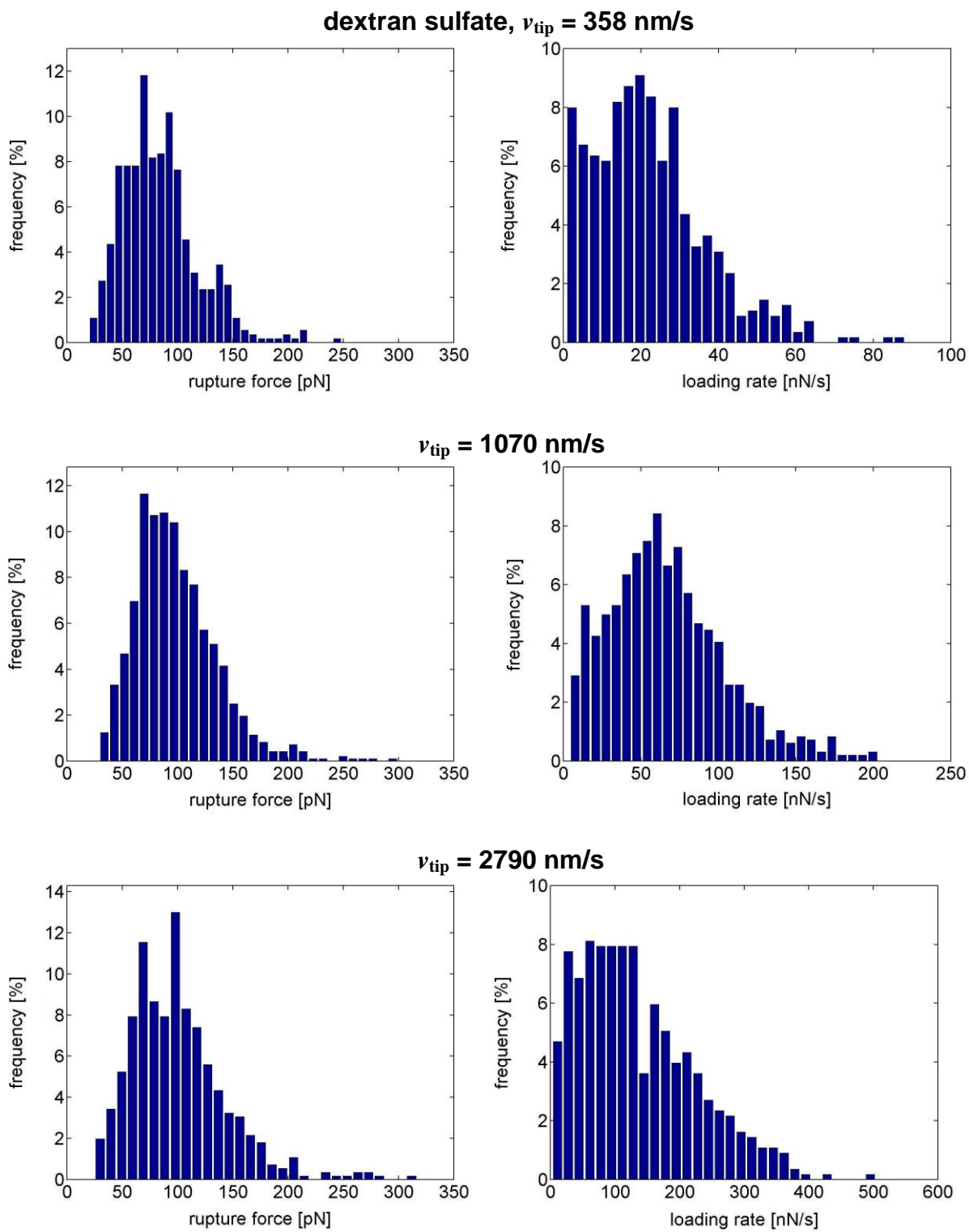


Fig. S12: Histograms of (**left column**) rupture force and (**right column**) loading rate distribution for the dextran sulfate/PF4-interaction, conducted at the tip retraction velocities v_{tip} as indicated in the figures. The loading rate shows always a broad distribution (containing small values even at large v_{tip}), making it necessary to group the measured events as described in the Materials and Methods section to extract meaningful values (the result can be found in Fig. S13).

dextran sulfate

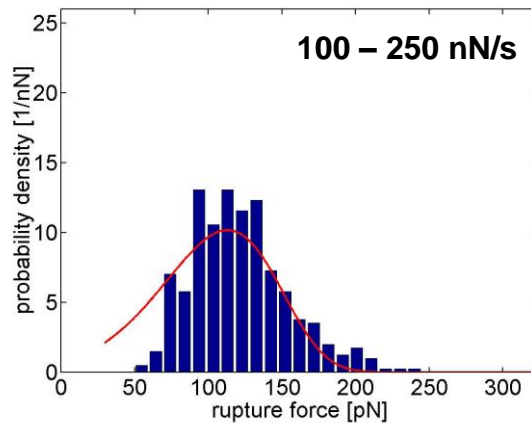
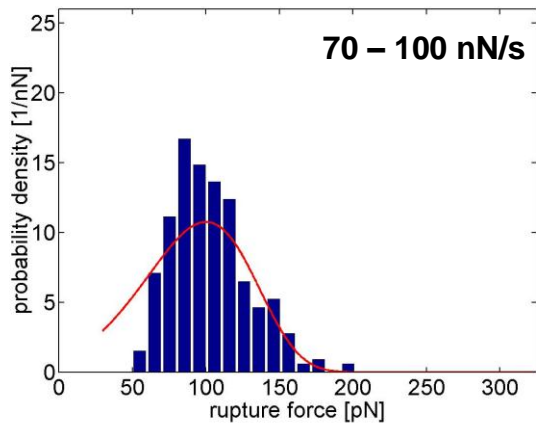
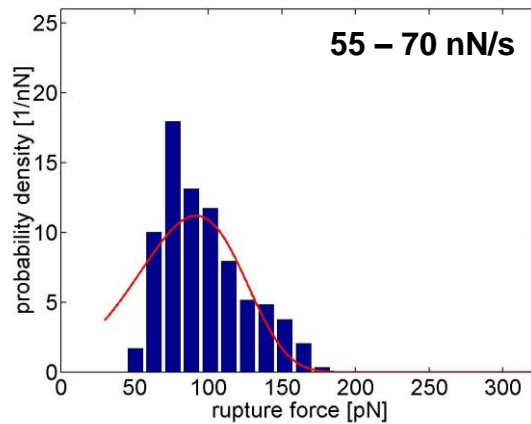
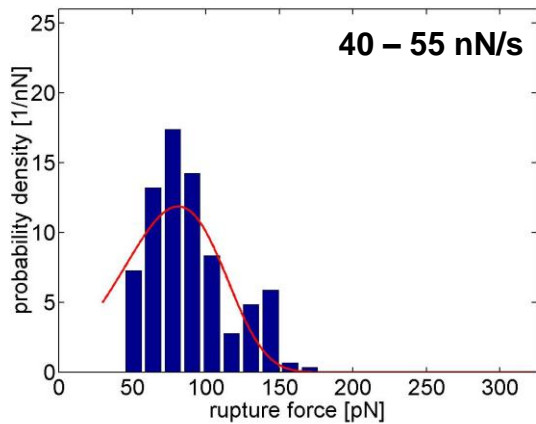
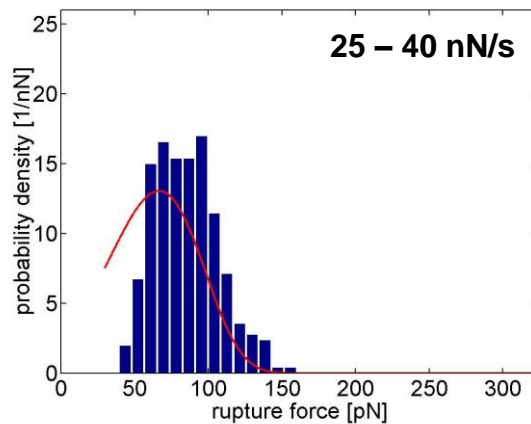
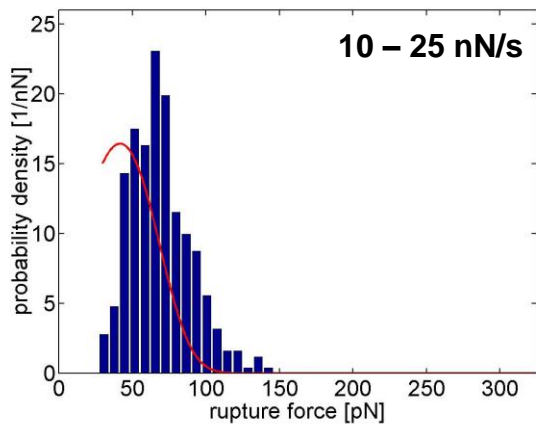


Fig. S13: Histograms of rupture force of the dextran sulfate/PF4-interaction after grouping the events according to the loading rate (as described in the Materials and Methods section). Shown are only the loading rate intervals that contained enough data points to plot a histogram. The red line gives the theoretically expected distribution of the rupture force $w(F_u)$ using the binding parameters of dextran sulfate (see Tab. S2) as described in Fig. S9 and S11. Minor deviations are found for low loading rates, while a very good agreement is observed for loading rates > 40 nN/s.